Eur. Phys. J. A **17**, 625–631 (2003)
DOI 10.1140/epja/i2003-10020-8

THE EUROPEAN PHYSICAL JOURNAL A

Muon capture on nickel and tin isotopes

N.T. Zinner[1], K. Langanke[1], K. Riisager[1,a], and E. Kolbe[2]

[1] Institute for Physics and Astronomy, University of Aarhus, DK-8000 Aarhus, Denmark
[2] National Cooperative for the Disposal of Radioactive Waste, Hardstrasse 73, CH-5430 Wettingen, Switzerland

Received: 28 January 2003 / Revised version: 7 March 2003 /
Published online: 4 June 2003 –
Communicated by J. Äystö

Abstract. We calculate total and differential muon capture rates on nickel and tin isotopes ranging from the proton dripline to the neutron dripline. The total rates decrease as the neutron number increases due to the combined effect of gradual blocking of available final-state neutron levels and of decreased phase space. The ordering of single-particle levels determines when blocking becomes important. We show that the total capture rates thereby are sensitive to the evolution of nuclear structure along an isotope chain.

PACS. 24.30.Cz Giant resonances – 23.40.-s Beta decay; double beta decay; electron and muon capture – 23.40.Hc Relation with nuclear matrix elements and nuclear structure

1 Introduction

Nuclear-structure physics and weak-interaction physics have since long been intertwined, weak interactions being used to study nuclei and nuclei being used in detailed tests of the weak interaction. The study of nuclei far from the line of beta-stability is nowadays a major subject within nuclear structure and it is therefore natural to ask how different weak-interaction probes can contribute to this study. Our aim in this paper is to investigate in detail the case of muon capture on nuclei. Muon capture on stable nuclei has been studied in detail for many years and is treated in several books and review papers [1–3]. The weak-interaction aspects of the captures will not change when going to unstable nuclei and most of the theoretical formalism can therefore be taken over unchanged. In this paper we calculate total capture rates and the final-state excitation spectrum for the isotope chains of Ni and Sn. Adding the information from a previous [4] calculation on the Ca chain, we discuss to what extent the measurements of these quantities can elucidate the nuclear-structure changes along the chains. Our results indicate that muon capture experiments should be considered at the next-generation radioactive beam facilities. Experimental investigation of nuclear muon capture can so far only be done on stable or long-lived isotopes, but the possibility of extending experiments to short-lived isotopes is being actively investigated at the moment (see, *e.g.*, [5,6]).

[a] e-mail: kvr@phys.au.dk

2 Model description

Our calculations are based on the random phase approximation (RPA) which, despite its simplicity, has been previously shown to describe muon capture on nuclei quite satisfactorily [7–9]. As in [8] we adopt an RPA which distinguishes between proton and neutron degrees of freedom for the particle and hole states, *i.e.* for muon capture our model changes a proton particle in the parent nucleus to a neutron hole state in the daughter. Our parent ground states are described by the lowest independent particle model state, assigning partial occupancy to the last shell if this is not completely occupied. The same shell is included among the hole states, but appropriately partially blocked [10]. The partial occupation formalism necessarily assumes a spin/parity assignment of $J^\pi = 0^+$ for the parent ground state. Therefore, we will restrict our studies in the following to even nickel and tin isotopes. The particle and hole states have been determined from a Woods-Saxon potential with the radius parameter taken as $1.22\,\mathrm{fm}\cdot A^{1/3}$, the diffuseness parameter a is 0.53 fm and the strength of the spin-orbit term V_{LS} is adjusted to give the correct spin-orbit splitting for p and f states (V_{LS} is -8.95 MeV for Ni and -9.00 MeV for Sn). The depth of the potential has been adjusted to reproduce the proton and neutron separation energies in the parent nucleus. If necessary, the neutron hole energies were slightly shifted to reproduce the Q-value of the reaction. As residual interaction we used the Landau-Migdal force given in [11]. As shown in [8], very similar results are obtained when using this force and a finite range force based on the Bonn potential

and therefore we do not expect the total muon capture rates to be sensitive to the chosen residual interaction. For the nuclear binding energies we adopted the experimental masses. If these were not known, we used the mass compilation of Goriely *et al.* [12].

In our calculations, we considered all multipole transitions with $\lambda \leq 4$ and both parities. From shell model calculations it is well established that the Gamow-Teller (GT) strength requires an additional quenching factor [13, 14] which we take from [15] as $(0.7)^2$. For the nickel isotopes ^{58,60,62,64}Ni the total strength is known experimentally (collected in [16]) and agrees well with the shell model results. For these nuclei we adjust our calculated GT strength to the data. Hence, the Ikeda sum rule is also modified by the same factor. For the other multipole operators, there exists no firm indication of a need for such additional quenching factors. For the q-dependence of the nuclear form factors we use the standard dipole form. We note that we adopt the appropriate multipole operators for finite momentum transfer [1]. Thus, only in the limit $q \to 0$ do our 0^+ and 1^+ operators reduce to the Fermi and Gamow-Teller operators, respectively. Nevertheless, for brevity we will in the following refer to the momentum-dependent 0^+ and 1^+ multipole operators as Fermi and Gamow-Teller operators.

The muon wave function in the atomic ($1s$) orbital has been derived by solving the Dirac equation for an extended charge distribution. In general, the RPA can lead to spurious center-of-mass excitations, which could mix with isoscalar transitions to 1^- states and thereby add artificial strength. As we solve the RPA eigenvalue problem in a complex model space, the center-of-mass contributions can be identified by their imaginary energy eigenvalue. We remove all states with dominating imaginary components, in this way also eliminating some of the real isoscalar 1^- strength. But as muon capture is dominated by isovector excitations, the eliminated strength is negligibly small and does not affect our calculated rates.

Muon capture also depends on the induced pseudoscalar hadronic weak current. At the free nucleon level the corresponding coupling constant is determined by the Goldberger-Treiman relation [17]

$$F_P(q^2) = \frac{2M_p F_A(0)}{m_\pi^2 - q^2} \ , \tag{1}$$

where m_π is the pion mass and $F_A(0) \equiv g_A = 1.25$. (In muon capture one often uses a dimensionless quantity $g_P = m_\mu F_P(q^2)$ at the relevant momentum transfer $q^2 \simeq -0.9 m_\mu^2$, such that $g_P \simeq 8.4$ for free protons.) In nuclear medium F_P can be again renormalized, and this renormalization does not necessarily obey the Goldberger-Treiman relation [18]. We have shown in our previous work that the total muon capture rates are not sensitive enough to the various choices of F_P renormalization. Consequently, throughout this work we use the Goldberger-Treiman relation.

3 Results

We have studied muon capture for even nickel and tin isotopes, spanning the range from the proton dripline (^{48}Ni, ^{100}Sn) to isotopes close to the (unknown) neutron dripline (^{86}Ni, ^{160}Sn) in both chains. The nickel isotope chain includes 3 double-magic nuclei (^{48}Ni, ^{56}Ni, ^{78}Ni), while the neutron magicity for ^{68}Ni is currently controversially discussed (*e.g.*, [19,20]). In the tin isotope chain, the nuclei ^{100}Sn and ^{132}Sn are identified as double-magic. For all nickel and tin isotopes a proton magicity is commonly accepted. This fact clearly eases a description of the muon capture process within an RPA formalism.

As benchmarks it is useful to recall the structure of the various isotopes within the independent particle model, which we adopt for the description of the uncorrelated parent ground state. For the nickel isotopes, the protons close the $f_{7/2}$ subshell. Between ^{48}Ni and ^{56}Ni, the neutrons fill the $f_{7/2}$ orbitals, while the rest of the (pf) shell is filled up to ^{68}Ni. The $g_{9/2}$ orbital is occupied in ^{78}Ni. For even heavier nickel isotopes, neutrons are moved into the $d_{5/2}$ and $s_{1/2}$ orbitals. On the basis of these simple structure considerations one observes that Fermi transitions are only possible in muon capture on even nickel isotopes up to ^{54}Ni, while Gamow-Teller transitions are Pauli blocked at ^{68}Ni. In the tin isotopes, the protons close the $g_{9/2}$ subshell. In ^{100}Sn the neutrons have the same configuration. Between ^{100}Sn and ^{120}Sn the neutrons fill the rest of the orbitals in the (gds) shell, followed by the $h_{11/2}$ intruder orbital, which is closed in ^{132}Sn. For heavier nuclei the neutrons occupy the other levels in the (hfp) shell. For all tin isotopes Fermi transitions are forbidden. The Gamow-Teller transitions are blocked, once the $g_{7/2}$ neutron orbitals are occupied, which happens, in our parametrization, for ^{114}Sn. We use the fact that the muon capture on ^{48,50,52,54}Ni allows Fermi transitions by adjusting the neutron hole energies in these nuclei such as to reproduce the Isobaric Analog State in the daughter.

For ^{58,60,62}Ni the muon capture rate is known experimentally [21]. Our calculated rates are 6.44×10^6 s^{-1} for ^{58}Ni, 5.18×10^6 s^{-1} for ^{60}Ni and 4.65×10^6 s^{-1} for ^{62}Ni. These results agree nicely with the data $(6.11(10) \times 10^6$ s^{-1}, $5.56(10) \times 10^6$ s^{-1} and $4.72(10) \times 10^6$ s^{-1} for ^{58}Ni, ^{60}Ni, ^{62}Ni, respectively). Our complete set of RPA results for the total muon capture rate on the nickel isotopes is plotted in fig. 1. It has long been recognized that the experimentally known muon capture rates are well described by a rather simple scaling rule. This Primakoff rule describes the capture rate Λ on a nucleus with mass number A and neutron number N as [22]

$$\Lambda(A,Z) = Z_{\rm eff}^4 X_1 \left(1 - X_2 \frac{(A-Z)}{2A}\right) . \tag{2}$$

Here, the second term in the parentheses corrects for Pauli blocking in a final nucleus with neutron excess. The use of an effective charge number $Z_{\rm eff}$ rather than Z accounts for corrections needed as the nuclear and muonic radii are comparable [3]. The parameters X_1, X_2 are determined to reproduce the trends of the capture rates on many

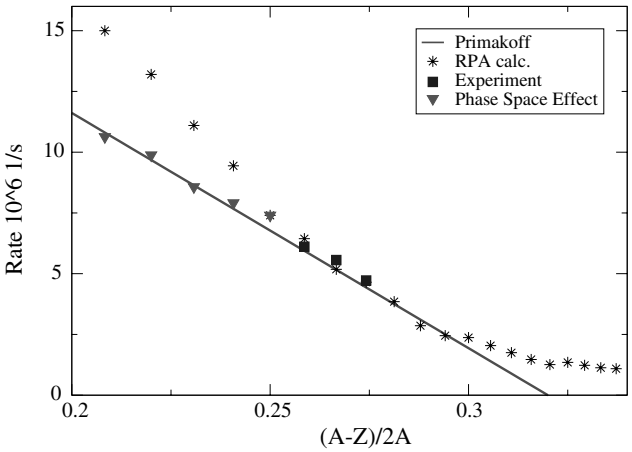

Fig. 1. The calculated total muon capture rate in even nickel isotopes (stars) is plotted *versus* $(A-Z)/2A$. The rates agree with experiment (boxes) for stable nuclei. The linear dependence expected from the Primakoff rule is violated for nuclei away from the line of stability, for proton-rich nuclei this is due to increased phase space (rates corrected for this are shown by triangles), for neutron-rich nuclei it is due to contributions from higher-order weak transitions.

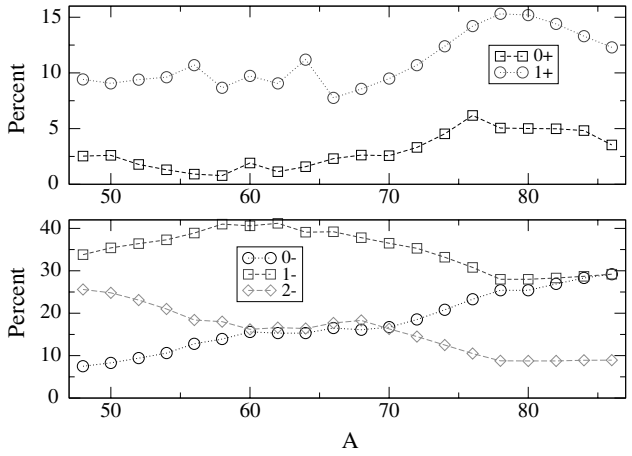

Fig. 2. Fractional contribution of different multipoles to the calculated total capture rate on even nickel isotopes. The top panel displays transitions of even parity ($0\hbar\omega$, $2\hbar\omega$), the bottom panel the ones of odd parity ($1\hbar\omega$, $3\hbar\omega$). See the text for a discussion of the trends visible.

beta-stable nuclei, reaching out to neutron excesses of $(A-Z)/A = 0.61$. Reference [21] gives these parameters as $X_1 = 170\ \mathrm{s}^{-1}$ and $X_2 = 3.13$. As is demonstrated in fig. 1, the Primakoff rule with this parametrization agrees quite nicely with our RPA results for the "non-exotic" nickel isotopes between ^{58}Ni and ^{68}Ni. However, for isotopes, which are more proton rich than ^{58}Ni or more neutron rich than ^{68}Ni, our calculations predict muon capture rates which are larger than predicted by the Primakoff parametrization to beta-stable nuclei. As we will now discuss, the reasons for these observed deviations are different for proton-rich and neutron-rich nuclei.

Figure 2 shows the various multipole contributions to the total muon capture rates on the nickel isotopes. As observed already previously for other nuclei (*e.g.*, [8,9,4]), muon capture is dominated by first-forbidden transitions, which account for nearly 70% of the total rate for all nickel nuclei. However, the relative weight among the 3 spin-dipole contributions ($J^\pi = 0^-, 1^-, 2^-$) changes significantly with increasing neutron number. We note that the relative contribution of the 0^- multipole increases within the nickel isotope chain from ^{48}Ni, while the 2^- contribution shows the opposite behavior. This behavior can be understood by looking at the excitation spectrum for these multipoles which is shown in fig. 3 for the 3 double-magic nickel isotopes. For ^{48}Ni there is a noticeable 2^- transition at low excitation energies ($E \sim 5$ MeV), which corresponds to a proton-neutron $d_{3/2} \rightarrow f_{7/2}$ single-particle transition, while the collective spin-dipole 2^- resonance is widely spread in energy ($E \approx 12$–28 MeV). Between ^{48}Ni and ^{56}Ni the neutron $f_{7/2}$ orbital gets filled. This blocks the $d_{3/2} \rightarrow f_{7/2}$ transition, which finally vanishes in ^{56}Ni. The main collectivity of this multipole centers now around the proton-neutron $f_{7/2} \rightarrow g_{9/2}, g_{7/2}$ excitations, centered in ^{56}Ni at excitation energies around $E \sim 8$ MeV and 18 MeV, where the difference reflects the spin-orbit splitting between the two g orbitals (which in our parametrization is nearly 10 MeV). In ^{78}Ni the $f_{7/2} \rightarrow g_{9/2}$ transition is blocked, thus the collectivity for the 2^- multipole now resides around one large ($f_{7/2} \rightarrow g_{7/2}$) transition at $E \sim 10$ MeV. The strength in ^{78}Ni between $E \approx 15$–30 MeV reflects already higher-order ($3\hbar\omega$) contributions. These higher-order transitions are also present in the other isotopes, but are here of less relative importance, as the first-forbidden transitions are larger. We also note that, with increasing neutron number, the multipole strength systematically moves to smaller excitation energies. This has been already observed and explained in [23]. The other first-forbidden multipoles can be understood by the same dominant collective transitions, where we note that the $d_{3/2} \rightarrow f_{7/2}$ single-particle transitions are not possible for $1^-, 0^-$ multipoles. This exclusive presence of $d_{3/2} \rightarrow f_{7/2}$ single-particle transitions in the 2^- multipole and its blocking when the neutron $f_{7/2}$ shell is getting filled, explains the relative decrease of the 2^- multipole rate between ^{48}Ni and ^{56}Ni. With respect to the collective transitions, we observe that for the 1^- multipole both proton-neutron $f_{7/2} \rightarrow g_{9/2}, g_{7/2}$ excitations are allowed, while the first is forbidden for the 0^- multipole. This explains why the relative 1^- contribution, analogously to the 2^- rate, decreases between ^{68}Ni and ^{78}Ni, when the $g_{9/2}$ neutron orbitals are filled. Such a blocking does not occur for the 0^- multipole, hence its relative importance increases for these nuclei. We again observe higher-order ($3\hbar\omega$) contributions to the capture rate, which, for the 1^- multipole becomes relatively important in isotopes heavier than ^{68}Ni.

We also observe that for the 1^- multipoles the two centroids of the collective transitions are shifted in energy relative to those of the 2^- multipole. This reflects the

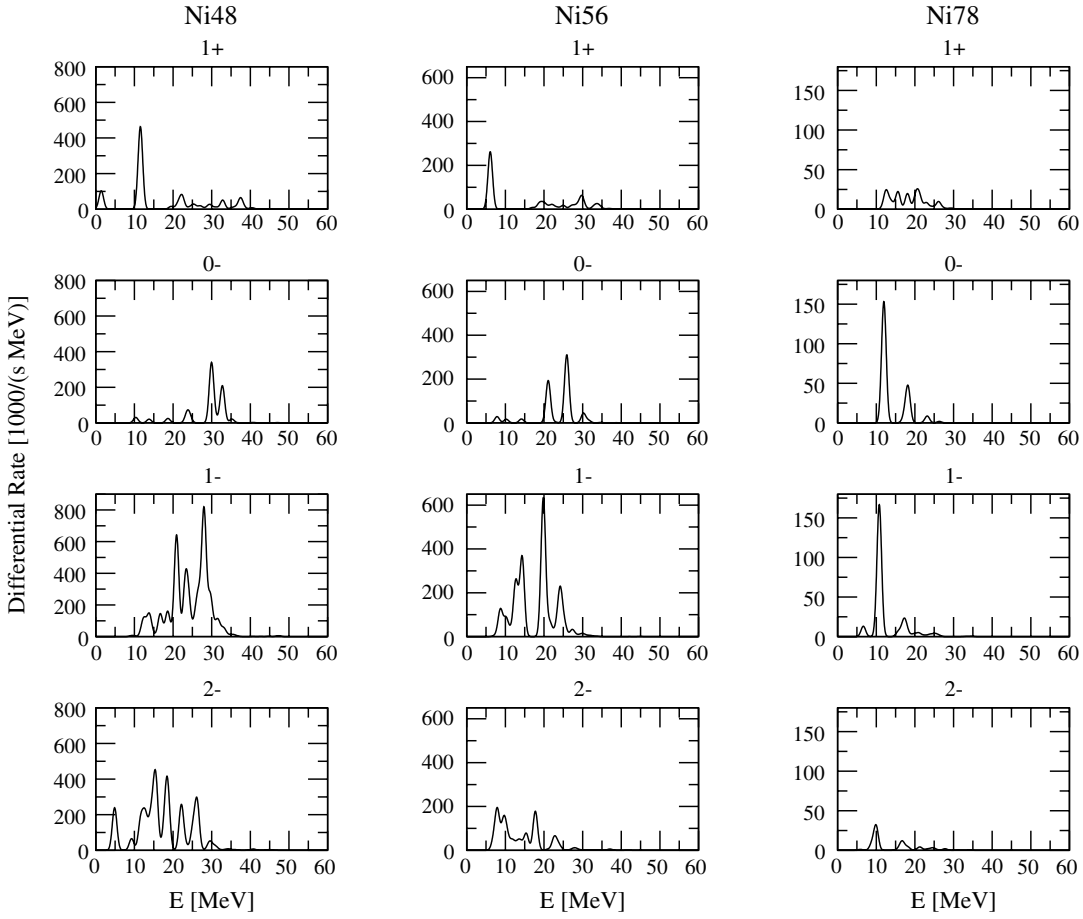

Fig. 3. Excitation spectra for the $J^\pi = 1^+, 0^-, 1^-, 2^-$ multipole operators for the three double-magic nickel nuclei ^{48}Ni, ^{56}Ni and ^{78}Ni. The RPA results have been folded with a Gaussian distribution of width 1 MeV.

effect of the RPA residual interaction [24], which lowers the 2^- centroids relative to the 1^-, 0^- centroids. For the 0^- multipole, only $f_{7/2} \rightarrow g_{7/2}$ transitions are possible.

Figure 3 also shows the excitation function for the 1^+ multipole. For ^{48}Ni, ^{56}Ni the main strength corresponds to the neutron-proton $f_{7/2} \rightarrow f_{5/2}$ transition, which gets blocked successively by filling of the (pf) shell in ^{68}Ni. In ^{48}Ni, the strength at $E \sim 2$ MeV corresponds to the $f_{7/2} \rightarrow f_{7/2}$ transition. Furthermore, we observe 1^+ strengths in this nucleus between 20 and 40 MeV, which is shifted to lower energies with increasing neutron excess. This strength reflects $2\hbar\omega$ transitions, which in nickel isotopes heavier than ^{68}Ni (*e.g.*, ^{78}Ni) dominate the 1^+ multipole as the $0\hbar\omega$ GT transitions are Pauli forbidden. We note here, that large-scale shell model calculations predict some correlation mixing of (pf) shell orbitals with the $g_{9/2}$ orbital which promotes about one neutron into the $g_{9/2}$ level for nuclei like ^{68,70}Ni [20], thus unblocking the GT transitions in these nuclei. However, the corrections of such transitions are too small to significantly change the conclusions drawn here.

Now we come back to the observation that our calculated muon capture rates for very proton-rich and neutron-rich nickel isotopes are significantly larger than the predictions of the Primakoff rule. The parameters for this scaling law correspond to the rates for the 3 stable nickel isotopes ^{58,60,62}Ni, for which data are available. This linear scaling law predicts the muon capture rate to vanish for nickel isotopes heavier than $A \sim 78$. Figure 1 shows that the simple linear scaling breaks down for $A > 68$ and that there is still a sizable muon capture rate for nickel isotopes heavier than ^{78}Ni. To understand this behavior we note that (see fig. 2) the rates for ^{58,60,62}Ni are dominated by the first-forbidden transitions and, moreover, there are no significant variations in the relative contributions of these multipoles between ^{58}Ni and ^{68}Ni as none of the dominant proton-neutron transitions for these multipoles are affected by the changes of the nuclear structure (*i.e.* filling of the (pf) shell neutron orbitals) in these isotopes. However, the $f_{7/2} \rightarrow g_{9/2}$ transitions, which contribute sizably to the data, are getting successively blocked beyond ^{68}Ni. For such nuclei the muon capture rate is dominated by the $f_{7/2} \rightarrow g_{7/2}$ transitions and the higher-order contributions to the first-forbidden (and the $0^+, 1^+$) multipoles, which all do not vanish, and are responsible for the deviations from the simple linear parametrization of the rates with neutron excess, as expected from the data determined for

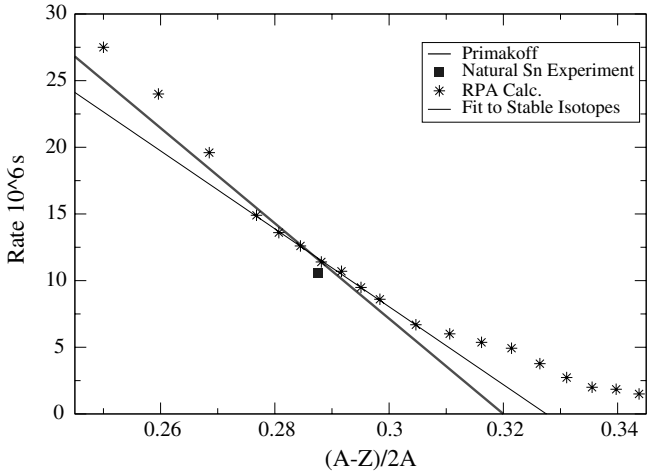

Fig. 4. As fig. 1, but for tin isotopes. Experimental data are only available for natural tin (box). The thin line is a linear fit to the calculated rates for stable tin isotopes.

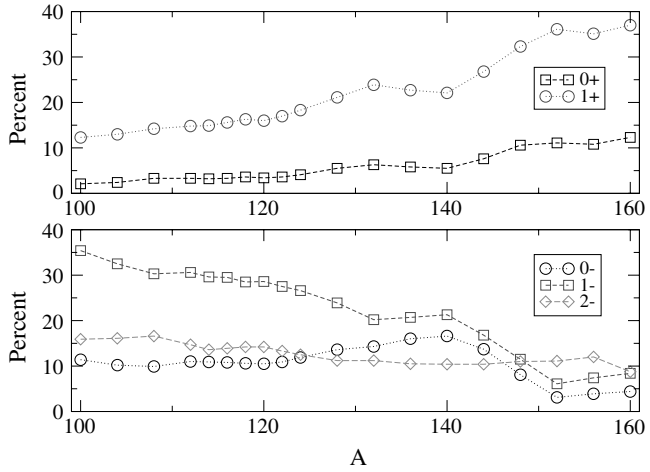

Fig. 5. As fig. 2, but for tin isotopes.

stable isotopes. It is noteworthy that the total capture rate on an extremely neutron-rich nucleus like ^{78}Ni is still about 20% of the rate on the stable isotopes ^{60,62}Ni.

Another quantity, which obviously affects the total rate, is the phase space, which scales like $\sim (m_\mu + Q - E_{\rm ex})^2$, where $m_\mu = 105.6$ MeV is the muon mass, Q the reaction Q-value and $E_{\rm ex}$ the nuclear excitation energy in the daughter nucleus. For the stable nickel isotopes Q is slightly negative ($Q = -0.38$ MeV, -2.88 MeV, -5.31 MeV for ^{58}Ni, ^{60}Ni, ^{62}Ni, respectively), while the average excitation energy can be estimated as $E_{\rm ex} \sim 15$–20 MeV in these nuclei. This leads to rather mild variations of the phase space for the stable isotopes. For more neutron-rich nuclei the Q-value gets increasingly more negative, which is counterbalanced somewhat by the average excitation energy, which moves to lower energies. For more proton-rich nuclei, the trend is opposite. Here, the nickel isotopes are unstable against electron capture, implying a positive Q-value, but the average excitation energy of the various multipole transitions is shifted upwards in excitation energies compared to the stable isotopes. However, the relevant difference $Q - E_{\rm ex}$ increases in these nuclei, enlargening the phase space for proton-rich nuclei compared to the stable ones. In fact, if we separate the dominating energy dependence of the phase space from the muon capture rate by multiplying the rate for the proton-rich nuclei with mass number A by $[(m_\mu + Q - E_{\rm ex})_A/(m_\mu + Q - E_{\rm ex})_{A=60}]^2$, the capture rates for these nuclei nicely follow the linear Primakoff scaling rule, as shown in fig. 1. This shows that the observed deviations of the rate for proton-rich nuclei from the linear rule are mainly phase space related and that nuclear-structure effects do not play a large role here.

As a second isotope chain we have studied the muon capture on the tin nuclei between the double-magic $N = Z$ nucleus ^{100}Sn and the extremely neutron-rich nucleus ^{160}Sn, which is close to the neutron dripline for this isotope chain. Our RPA results for the total muon capture rates are summarized in fig. 4. Experimentally the capture rate is known for natural tin: $\Lambda = 10.6 \times 10^6$ s^{-1}. This agrees very nicely with our estimate of $\Lambda_{\rm th} = 11.2 \times 10^6$ s^{-1}, which we have obtained by averaging our RPA rates Λ_i for the stable tin isotopes, *i.e.* $\Lambda_{\rm th} = \sum_i a_i \Lambda_i$ where the index i runs over $i = 112, 114, 115, 116, 117, 118, 119, 120, 122, 124$ and a_i is the percentage of the respective isotope in natural tin. (The rates for odd-A isotopes have not been calculated, but are extrapolated from the linear fit given below. They only contribute 17% to the weighted rate and are not expected to change the estimate appreciably). The standard Primakoff parametrization gives a reasonable fit to our tin muon capture rates. We note that the RPA results for the stable isotopes follow nearly perfectly the straight line of eq. (2) if the two parameters are slightly modified from their standard values; a fit with $X_1 = 181.2$ and $X_2 = 3.05$ is also shown in fig. 4.

Like for the nickel isotopes, we observe that the calculated muon capture rates for the proton-rich (*i.e.* $A < 112$) and neutron-rich (*i.e.* $A > 132$) nuclei are larger than predicted by the linear Primakoff parametrization(s). The reasons are the same as identified for the nickel isotopes.

Our muon capture rates on the tin isotopes are broken down into the dominant multipole contributions in fig. 5. The first-forbidden transitions contribute around 60% of the rate for the tin isotopes lighter than ^{132}Sn. For heavier isotopes the 0^+ and, in particular, the 1^+ transitions become increasingly important and, for $A > 140$ they supply a larger portion of the total capture rate than the first-forbidden transitions. We note that the partial $0^+, 1^+$ rates correspond to $2\hbar\omega$ transitions, as the allowed GT proton-neutron $g_{9/2} \rightarrow g_{7/2}$ transitions are essentially Pauli blocked for tin isotopes beyond $A = 114$. However, the $2\hbar\omega$ multipoles are virtually unaffected when the $(h_{9/2} i_{13/2} fp)$ neutron orbitals get filled beyond ^{132}Sn. This is, of course, different for the first-forbidden transitions. At first, the $h_{11/2}, s_{1/2}, d_{5/2}$ neutron orbitals are rather close in energy and hence strongly mixed in the tin isotopes ^{114}Sn to ^{132}Sn. The associated blocking of the $g_{9/2} \rightarrow h_{11/2}$ transitions reduces the relative partial

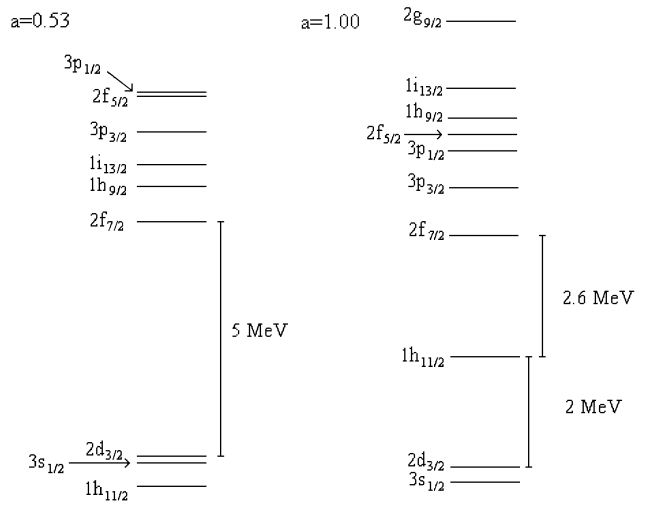

Fig. 6. The single-particle level ordering in our model for neutron levels relevant for the tin isotope chain is shown for two values of the diffuseness parameter, $a = 0.53$ fm and 1.0 fm.

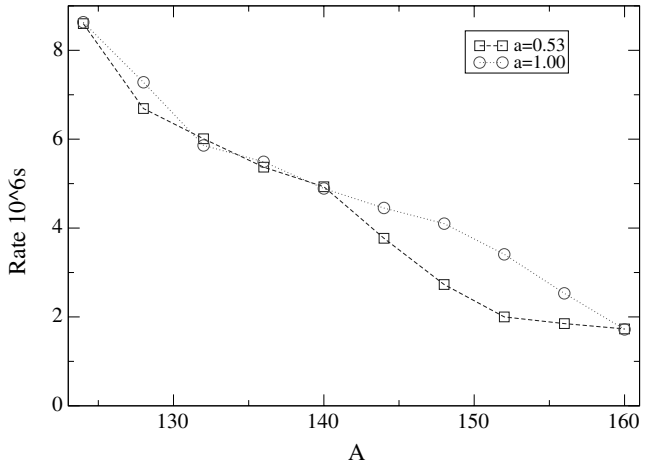

Fig. 7. The total muon capture rates calculated for the neutron-rich tin isotopes are shown for two different values of the diffuseness parameter, $a = 0.53$ fm and 1.0 fm. As explained in the text the difference between the two calculations is related to the different single-particle level ordering (see fig. 6).

$1^-, 2^-$ rates. A similar blocking in the $0^-, 1^-$ multipoles, now related to the $g_{9/2} \rightarrow h_{9/2}$ transition is observed in the isotopes beyond $A > 140$, for which the neutron levels $h_{9/2}, i_{13/2}, p_{3/2}$ are strongly mixed.

In a seminal paper, Dobaczewski *et al.* [25] pointed out that in very neutron-rich nuclei a neutron skin might develop increasing the diffuseness of the nuclear surface. As a consequence, the spin-orbit potential, whose radial dependence is proportional to the derivative of the central Woods-Saxon potential, should be reduced in neutron-rich nuclei. Such a reduction will significantly affect the single-particle structure in these nuclei. It is speculated that in very neutron-rich nuclei the shell structure might resemble again the one of the harmonic oscillator rather than the one of an oscillator with a strong spin-orbit splitting, as encountered for stable nuclei. We have explored which effects a change of the diffuseness parameter and, relatedly, of the spin-orbit potential has on the muon capture rates for very neutron-rich tin isotopes. Guided by ref. [25] we adopt the diffuseness parameter to $a = 1.0$ fm, rather than our standard value of $a = 0.53$ fm. The resulting changes in the single-particle structure are shown in fig. 6. Clearly, the reduction of the spin-orbit potential moves the $h_{11/2}$ orbit up in energy compared to the $d_{3/2}, s_{1/2}$ orbitals. While for $a = 0.53$ fm these 3 orbitals are nearly degenerate and a strong shell gap develops to the $f_{7/2}$ orbital, the $h_{11/2}$ orbital moves between the two adjacent shells for the larger diffuseness parameter. For the following discussion, however, it is more important, that the $h_{9/2}$ and $i_{13/2}$ orbitals are also pushed up in energy. In particular, we find the p orbitals and the $f_{5/2}$ orbital below the $h_{9/2}$ orbitals for the Woods-Saxon parametrization with $a = 1.0$ fm. The consequences for the muon capture rates are shown in fig. 7. The capture rate for the tin isotopes between ^{140}Sn and ^{160}Sn is noticeably larger for $a = 1.0$ fm than for $a = 0.53$ fm. The reason is as follows: For the $a = 0.53$ fm parametrizations, the neutron $h_{9/2}$ levels are filled for the isotopes between $A = 140$ and 150. This strongly blocks the proton-neutron $g_{9/2} \rightarrow h_{9/2}$ transitions, which dominate the first-forbidden responses and reduces the capture rates. However, for $a = 1.0$ fm the blocking of these dominant transitions occurs for the isotopes $A > 152$. As a consequence, the total muon capture rates are predicted to be noticeably larger for tin isotopes $A \sim 145$, if the development of a neutron skin occurs and leads to the reduction of the spin-orbit potential. This conclusion ties in very well with our explanation above of how the capture rate develops in general with neutron excess and it underlies that accurate measurements of the rate can be sensitive to the development of nuclear structure.

4 Discussion

Already the previous calculations on muon capture on calcium isotopes [4] showed that extrapolation to unstable nuclei of the Primakoff formula fitted to stable nuclei gives a bad fit. However, the range of isotopes investigated there was more limited than what is possible for nickel and tin, and the results obtained here point in a much more direct way to the filling of orbits as the crucial ingredient in understanding the development of capture rates with neutron number. With proper account taken for the effective charge $Z_{\rm eff}$ we would expect to see similar effects when varying instead the proton number in an isotone chain.

The dependence on the neutrino phase space, that explains the deviation from the simple Primakoff rule for proton-rich nuclei, cf. fig. 1, is included in the original formulation of the rule [22]. Since the derivation explicitly assumed that the contributions from higher multipoles (d-waves and above for the outgoing neutrino) are small, it is also not surprising that the formula fails for very neutron-rich nuclei. Reviews of nuclear muon capture consistently point out that the rates fluctuate systematically

even for stable nuclei [2,21,3], but we have not encountered earlier suggestions for how these systematic fluctuations are related to nuclear-structure questions. We note that measurements of the capture rates for the individual stable tin isotopes could be interesting, since the rates are predicted to decrease linearly with $(A-Z)/2A$ with a slope slightly different from the one obtained in the global fit in [21]. However, to clearly see the effects from filling of different orbits one probably needs to include data from several stable isotope series or to include also unstable isotopes (the latter would give a more unambiguous test).

It might nevertheless be valuable to have an approximate formula that could be used for a rough prediction of capture rates over larger regions of the nuclear chart. By combining non–energy-weighted and energy-weighted sum rules Goulard and Primakoff [26] derived the following more complex fitting formula:

$$\Lambda(A,Z) = Z_{\rm eff}^4 G_1 \Bigg[1 + G_2 \frac{A}{2Z} - G_3 \frac{A-2Z}{2Z} - G_4 \left(\frac{A-Z}{2A} + \frac{|A-2Z|}{8AZ} \right) \Bigg]. \quad (3)$$

(The absolute signs in the last term are often neglected when treating only stable nuclei, but will be important in the general case.) This expression should include higher-order contributions as well as take the neutrino phase space into account. We have fitted this expression to the calculated values for the Ca, Ni and Sn chains from the present paper and ref. [4]. The four parameters turn out to be statistically very correlated, *i.e.* many different parameter sets will give an identically good fit to the rates, so we have somewhat arbitrarily (but guided by the best fit in [3]) put $G_3 = 0$ and get for the other parameters $G_1 = 168, G_2 = 0.40, G_4 = 4.71$. With these parameters the Goulard-Primakoff formula reproduces the calculated rates within a factor 2, typically better (it is clear from fig. 7 that we cannot expect a much better fit due to local nuclear-structure effects), although with a tendency to underestimate the rates for proton-rich nuclei. It could therefore be used for a first guess for capture rates for neutron-rich nuclei, at least for nuclei between Ca and Sn.

We have here only treated even-even nuclei. There is a known [3] odd-even Z effect in total capture rates, so the extension to odd-even and odd-odd systems might also turn out to give structure information. It might also be interesting to look at nuclei away from magic numbers where the occupancy numbers for the single-particle levels are more smeared out. It is not clear to what extent this could wash out the structure effects we have found here. More involved theoretical models are probably needed for such investigations.

In conclusion, our results indicate that interesting nuclear-structure information, namely the filling sequence of different orbits, might be probed even from the very simplest measurement on muon capture on unstable nuclei, that of the total muon capture rate. Even more information would be available if experiments could proceed a step further and measure the differential rates, but this has only been done in a quite limited way so far on stable isotopes [3] and will take longer to accomplish.

References

1. J.D. Walecka in *Muon Physics II*, edited by V.W. Hughes, C.S. Wu (Academic Press, New York, 1975) p. 113.
2. N.C. Mukhopadhyay, Phys. Rep. C **30**, 1 (1977).
3. D.F. Measday, Phys. Rep. **354**, 243 (2001).
4. E. Kolbe, K. Langanke, K. Riisager, Eur. Phys. J. A **11**, 39 (2001).
5. P. Strasser, T. Matsuzaki, K. Nagamine, Hyperfine Interact. **119**, 317 (1999).
6. K. Riisager, Eur. Phys. J. A **15**, 75 (2002).
7. Nguyen Van Giai, N. Auerbach, A.Z. Mekjian, Phys. Rev. Lett. **46**, 1444 (1981); N. Auerbach, A. Klein, Nucl. Phys. A **422**, 480 (1984).
8. E. Kolbe, K. Langanke, P. Vogel, Phys. Rev. C **50**, 2576 (1994).
9. E. Kolbe, K. Langanke, P. Vogel, Phys. Rev. C **62**, 055502 (2000).
10. D. Rowe, Rev. Mod. Phys. **40**, 153 (1968).
11. K. Nakayama, S. Drozdz, S. Krewald, J. Speth, Nucl. Phys. A **470**, 573 (1987).
12. S. Goriely, F.T. Tondeur, J.M. Pearson, At. Data Nucl. Data Tables **77**, 311 (2001).
13. B.H. Wildenthal, Prog. Part. Nucl. Phys. **11**, 5 (1984).
14. K. Langanke, D.J. Dean, P.B. Radha, Y. Alhassid, S.E. Koonin, Phys. Rev. C **52**, 718 (1995).
15. G. Martinez-Pinedo, A. Poves, E. Caurier, A.P. Zuker, Phys. Rev. C **53**, R2602 (1996).
16. E. Caurier, K. Langanke, G. Martinez-Pinedo, F. Nowacki, Nucl. Phys. A **653**, 439 (1999).
17. M.L. Goldberger, S.B. Treiman, Phys. Rev. **111**, 354 (1958).
18. J. Delorme, M. Ericson, Phys. Rev. C **49**, R1763 (1994).
19. H. Grawe, M. Lewitowicz, Nucl. Phys. A **693**, 116 (2001).
20. O. Sorlin *et al.*, Phys. Rev. Lett. **88**, 092501 (2002).
21. T. Suzuki, D.F. Measday, J.P. Roalsvig, Phys. Rev. C **35**, 2212 (1987).
22. H. Primakoff, Rev. Mod. Phys. **31**, 802 (1959).
23. I. Hamamoto, H. Sagawa, X.Z. Zhang, Phys. Rev. C **57**, R1064 (1998).
24. T. Suzuki, Nucl. Phys. A **687**, 119c (2001).
25. J. Dobaczewski, I. Hamamoto, W. Nazarewicz, J.A. Sheikh, Phys. Rev. Lett. **72**, 981 (1994).
26. B. Goulard, H. Primakoff, Phys. Rev. C **10**, 2034 (1974).